

A treatment of the leading edge discontinuity for time-marching throughflow analyses

Simone Rosa Taddei¹, Francesco Larocca¹, Francesco Bertini²

¹*Department of Aerospace Engineering, Politecnico di Torino, Italy*

E-mail: simone.rosataddei@polito.it, francesco.larocca@polito.it

²*Avio Group, Italy*

E-mail: francesco.bertini@aviogroup.com

Keywords: turbomachinery axisymmetric model, blade force peak, inverse problem.

SUMMARY. An axisymmetric model for complete axial-flow turbomachines is adopted, which replaces the blades with hub-to-tip streamsurfaces. Axisymmetric Euler equations contain blockage and blade force terms that model the effects of the real blades on the flow. These equations are integrated to convergence by means of an upwind finite-volume scheme. An inverse problem is solved in the front part of the meridional blade regions, where a smooth swirl profile, instead of the detailed streamsurface geometry, is specified. This profile interpolates the swirl of the incoming flow and that imposed by the hub-to-tip streamsurface, with the purpose of removing the discontinuity due to non-zero incidence angles. In the interpolation region, the inviscid or normal component of the blade force is updated according to the specified swirl distribution and to the modified streamsurface geometry that produces it. The method does not change the blade load. Even with strong incidence angles, the method removes 99.9% of the numerical losses in mass flowrate and blade load. It allows meridional analysis of machines working in off-design conditions.

1 INTRODUCTION

Despite the increasing computational resources, full three-dimensional flow simulations based on computational fluid dynamics (CFD) methods are still far from being routinely used for the analysis and optimization of new, complete multistage turbomachinery. Throughflow or axisymmetric tools are still considered as the backbone of the aerodynamic design process by the most aeroengine companies [1]. These models take into account a single, mean hub-to-tip streamsurface, i.e. the blade cambersurface in the blade regions. Over the past 15 years, several CFD-based throughflow models, which involve time-marching solutions of Euler or Navier-Stokes equations in the meridional plane of the complete machine, have been proposed. In the axisymmetric flow equations, the main effects of the real blades on the flow are modelled by means of blade-to-blade blockage and blade force terms. Compared to the classical streamline curvature (SLC) and streamfunction (SF) methodologies, CFD-based approaches provide a more complete and physically-consistent description of the flowfield through the blade rows. In particular, they allow the detailed geometry of the blade cambersurfaces to be designed (by inverse solvers) or analyzed (by direct solvers) from the axisymmetric stage of the design process, at the cost of a single, two-dimensional CFD computation.

Because of the axisymmetry assumption, which is the basis of any throughflow model, the flow prerotation upstream of a blade row cannot be predicted. Whenever the incoming flow angle does not match the inlet blade angle, i.e. the incidence angle is non-zero, a discontinuity occurs at the leading edge. This discontinuity is associated with a blade force peak, which often leads to unacceptable numerical losses. In inverse/design formulations, where a particular flow quantity is specified in the

blade regions and the cambersurface geometry that realizes it is searched for, a simple way of overcoming the problem is to specify a suitable distribution of this quantity in the leading edge region. In direct/analysis formulations, where the cambersurface geometry is given, the leading edge needs an *ad hoc* treatment, but despite of its importance, up to now the problem has not been investigated very much. Reference [2] has suggested a modification of the flux balance at the blade inlet, in order to instantaneously turn the flow with no entropy production. Reference [3] has proposed to arbitrarily modify the front part of the blade, so that it can fit the direction of the incoming flow. The same approach has been followed in reference [4]. This work interestingly shows that turning the flow by means of a blade force always involves a numerical entropy production. This production is related to the quantity $\frac{\partial\alpha}{\partial m}$, i.e. the variation of the blade angle along the meridional streamlines, or the blade curvature. Whenever the leading edge is not aligned with the incoming flow, it behaves as a singularity where $\frac{\partial\alpha}{\partial m} = \infty$ and theoretically generates an infinite force. With the exception of the linear cascade case, the method adopted in references [3] and [4] does not seem much practical. However, its effectiveness has only been proved for small incidence angles.

In this work, a new approach has been followed. The method has been implemented in the frame of a Euler throughflow solver, but it is also valid for Navier-Stokes axisymmetric equations. Instead of adopting a pseudo-time technique as done in references [3, 4, 5], the present throughflow solver works more similarly to those of references [6, 7]. In the blade regions, the tangential momentum equation is not integrated. It is simply used to compute the tangential component of the inviscid or normal blade force field, once the swirl, i.e. the axial angular momentum, has been obtained from a cambersurface-flow slip equation. This approach allows the model to easily switch from the direct formulation to an inverse formulation where the swirl, instead of the cambersurface geometry, is specified. In the leading edge region, the swirl is specified as a convenient interpolation between that of the incoming flow and that of the first point where the slip equation is actually enforced. The underlying idea is to spread the blade force peak on an enough high point number, to make the numerical loss production at the leading edge comparable to that inherently involved by the numerical scheme. In order to fit the specified swirl distribution, a modification of the front part of the cambersurface is still needed, but this is now provided by the slip equation itself, consistently with the inverse approach. Handmade modifications are no longer done.

The following Section starts with a review of the time-marching throughflow model adopted by the authors. Section 3 goes into the details of the proposed leading edge treatment. Section 4 presents two simple test cases, dealing with i) a linear flat plate cascade, for which the theoretical solution is available for comparison with numerical results, and ii) a three-stage compressor analyzed in off-design conditions. Finally, some concluding remarks are given.

2 FRAMEWORK: THE EULER THROUGHFLOW MODEL

The axisymmetric model adopted by the authors shares the same basic idea as classical throughflow models, where the blade-to-blade or S1 streamsurfaces are revolutionary surfaces for the x axis and all the hub-to-tip or S2 streamsurfaces can be obtained by a rigid rotation of a single or mean surface around the same axis (Figure 1 left). In the blade regions, this mean surface can be thought of as the cambersurface of the blade. The direct or analysis formulation of the Euler solver computes the axisymmetric flowfield for a given, steady geometry $\bar{S}_2(x, r)$ of the blade cambersurfaces. Therefore, each of the S2 streamsurfaces will be identified by a different value of the constant in equation

$$S_2 = \vartheta - \bar{S}_2 = \text{const}$$

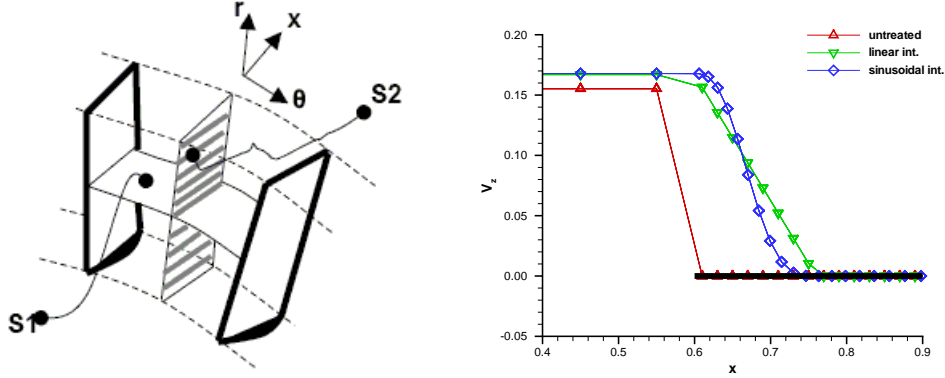


Figure 1: Blade-to-blade S1 and hub-to-tip S2 streamsurfaces (left); tangential speed on the flat plate cascade (right).

and, according to the definition of a streamsurface, will be tangent to the flow motion relative to the blade:

$$(\vec{V} - \omega r \vec{k}) \cdot \nabla S_2 = 0 \quad (1)$$

Axisymmetric Euler equations, written in non-dimensional terms for a cylindrical, inertial frame of reference, have the form

$$\frac{\partial}{\partial t} \begin{Bmatrix} \rho \\ \rho V_x \\ \rho V_r \\ \rho V_\vartheta \\ \rho E^0 \end{Bmatrix} + \frac{\partial}{\partial x} \begin{Bmatrix} \rho V_x \\ p + \rho V_x^2 \\ \rho V_x V_r \\ \rho V_x V_\vartheta \\ \rho V_x H^0 \end{Bmatrix} + \frac{\partial}{\partial r} \begin{Bmatrix} \rho V_r \\ \rho V_r V_x \\ p + \rho V_r^2 \\ \rho V_r V_\vartheta \\ \rho V_r H^0 \end{Bmatrix} + \frac{1}{r} \begin{Bmatrix} \rho V_r \\ \rho V_r V_x \\ \rho(V_r^2 - V_\vartheta^2) \\ 2\rho V_r V_\vartheta \\ \rho V_r H^0 \end{Bmatrix} = \begin{Bmatrix} \{Q_i\} \\ \{Q_v\} \\ \{Q_h\} \end{Bmatrix} \quad (2)$$

The source terms on the right side model the effects of the real blades on the flow. The term $\{Q_i\} = (0 \ f_{ix} \ f_{ir} \ f_{i\vartheta} \ f_{i\vartheta} \ \omega r)^T$ introduces the inviscid blade force field \vec{f}_i , which can be thought of as a redistribution of the pressure forces exerted by the blades on the entire blade-to-blade channel. Therefore, it will act normal to the S2 streamsurfaces:

$$\vec{f}_i \times \nabla S_2 = 0 \quad (3)$$

The term $\{Q_v\} = (0 \ f_{vx} \ f_{vr} \ f_{v\vartheta} \ f_{v\vartheta} \ \omega r)^T$ introduces the viscous blade force field

$$\vec{f}_v = -f_v \frac{\vec{V}_{rel}}{V_{rel}} = \frac{\cos \alpha_{rel}}{(1 + \frac{\gamma-1}{2} Ma_{rel}^2)^{\frac{\gamma}{\gamma-1}}} \frac{\partial p_{rel}^0}{\partial m} \frac{\vec{V}_{rel}}{V_{rel}} \quad (4)$$

which models the profile loss effects through a distributed loss [8]. This second force field is assumed to act in the direction opposite to the relative flow motion, i.e. tangential to the S2 surfaces. Finally, the term $\{Q_h\} = -\frac{\vec{V} \cdot \nabla h}{h} \rho (1 \ V_x \ V_r \ V_\vartheta \ H^0)^T$ models the blade-to-blade blockage effects for a given $h = 1 - \frac{n\delta_\vartheta(x,r)}{2\pi}$.

Since $d\bar{S}_2 = d\vartheta$ on a S2 streamsurface, slip equation (1) can be written in the form

$$V_x \frac{\partial \vartheta}{\partial x} + V_r \frac{\partial \vartheta}{\partial r} = \frac{1}{r^2} (rV_\vartheta) - \omega \quad (5)$$

whereas vector equation (3) gives rise to equations

$$f_{ix} = -r \frac{\partial \vartheta}{\partial x} f_{i\vartheta} \quad f_{ir} = -r \frac{\partial \vartheta}{\partial r} f_{i\vartheta} \quad (6)$$

Outside the blade regions, \vec{f}_i (and also \vec{f}_v) is zero and the system of equations (2) is sufficient to close the axisymmetric problem. In the blade regions, \vec{f}_i has to be determined by adding equations (5) and (6) to the system. The numerical time-marching procedure implemented in the throughflow code works similarly to those of references [6, 7]. The fourth of equations (2) is not integrated in the blade regions. The authors point out that it can be rewritten as a quasi-linear equation for the swirl, or axial angular momentum:

$$\frac{\partial (rV_\vartheta)}{\partial t} + \vec{V}_m \cdot \nabla (rV_\vartheta) = r \frac{f_{i\vartheta} + f_{v\vartheta}}{\varrho} \quad (7)$$

At each computational step, slip equation (5) provides a new swirl distribution. This distribution is introduced into the steady equation (7) to update $f_{i\vartheta}$. The other two components of the inviscid blade force field are updated by means of equations (6). In equation (7), $f_{v\vartheta}$ is provided by the distributed-loss equation (4) for a given erosion of the relative total pressure along the meridional streamlines. The overall total pressure drop between blade leading and trailing edge can be obtained from experimental profile loss correlations.

2.1 Numerical method

Euler equations are integrated to convergence through a finite-volume upwind scheme. The convective part of the equations is treated by a flux difference splitting method, with an approximate solution of the Riemann problem at each cell interface [9]. The scheme follows the guidelines of the Essentially Non-Oscillatory (ENO) approach [10]. It is second-order accurate both in space and in time, with linear reconstruction of the solution inside each cell through minmod limiters. Total quantities, ramp flow angle and blade-to-blade flow angle are prescribed along the inlet section of the machine, whereas the static pressure, ruled by a simple radial equilibrium equation, is prescribed along the outlet section. Finally, a slip condition is coupled to Euler equations along the endwalls.

3 METHOD: THE INVERSE SOLUTION IN THE LEADING EDGE REGION

The direct formulation of the throughflow model addressed in Section 2 can be easily turned into an inverse formulation where the swirl, instead of the cambersurface geometry, is specified in the blade regions. References [6, 7] have followed this approach to design the blade cambersurfaces for a target spanwise distribution of the specific rotor work.

Here, the inverse solution is only used in the front part of the blade with the purpose of smoothing the leading edge discontinuity in analysis computations. A convenient interpolation between the swirl in the last point downstream of the blade and that of the first point where slip condition (5) is actually used can be always specified. Two different choices will be compared in Section 4.1. The tangential component of the inviscid blade force field is still updated from equation (7), as in the remainder of the blade region. The authors point out that such a modification of the swirl profile

does not affect the blade load. This statement can be rigorously proved for a linear, infinite-span cascade with no loss effects. In this simple model, the throughflow approximation $\frac{\partial}{\partial z} = 0$ leads to

$$F_{iz} = - \int_{x_{1e}}^{x_{te}} h(x) f_{iz}(x) dx = \dot{m} \Delta V_z \quad (8)$$

where the mass flowrate, $\dot{m} = \rho V_x h = \text{const}$, and the tangential velocity jump between cascade inlet and outlet, ΔV_z , only depend on the boundary conditions, inlet flow angle and outlet blade angle [11]. Therefore, different $V_z(x)$ profiles, with ΔV_z kept constant, involve different $f_{iz}(x)$ distributions without changing integral (8).

The new velocity field in the leading edge region does not satisfy equation (5). Therefore, $\frac{\partial \vartheta}{\partial x}$ and $\frac{\partial \vartheta}{\partial r}$ can be no longer introduced into equations (6) to update f_{ix} and f_{ir} . Equation (5) is used to modify the front part of the blade cambersurface and fit the specified swirl distribution. In the computational plane $\xi\eta$ it takes the form

$$v_\xi \frac{\partial \vartheta}{\partial \xi} + v_\eta \frac{\partial \vartheta}{\partial \eta} = \frac{1}{r^2} (rV_\vartheta) - \omega \quad (9)$$

where

$$\begin{pmatrix} v_\xi \\ v_\eta \end{pmatrix} = \begin{bmatrix} \frac{\partial \xi}{\partial x} & \frac{\partial \xi}{\partial r} \\ \frac{\partial \eta}{\partial x} & \frac{\partial \eta}{\partial r} \end{bmatrix} \begin{pmatrix} V_x \\ V_r \end{pmatrix} \quad (10)$$

are the covariant components of the meridional velocity. The new coordinates ξ and η are streamwise and spanwise oriented, respectively. In particular, the inlet and outlet sections and all the leading and trailing edge sections are grid iso- ξ lines, whereas the hub and tip are grid iso- η lines. If meridional streamlines are assumed to follow, as a first approximation, grid iso- η lines, the cambersurface geometry only has to be modified in the ξ direction. At each computational step, the new geometry, $\vartheta'(\xi, \eta)$, will satisfy the following properties:

1. $\frac{\partial \vartheta'}{\partial \eta} = \frac{\partial \vartheta}{\partial \eta}$;
2. $\frac{\partial \vartheta'}{\partial \xi}$ is given by equation (9) with the specified rV_ϑ .

The new derivatives $\frac{\partial \vartheta'}{\partial x}$ and $\frac{\partial \vartheta'}{\partial r}$ that have to be introduced into equations (6) will be simply obtained by pre-multiplying $(\frac{\partial \vartheta'}{\partial \xi} \quad \frac{\partial \vartheta'}{\partial \eta})^T$ by the transpose of matrix (10). In the spirit of reference [4], the modification of the cambersurface geometry is only used for the computation of the inviscid blade force. The angle used for the empirical loss correlations is still the real blade angle.

Table 1: Comparison between theoretical and numerical results for the flat plate cascade.

	ρV_x	F_{iz}	F_{ix}
theoretical	0.42258	0.07094	-0.01299
untreated	0.39588	0.06137	0
linear int.	0.42069	0.07024	-0.01205
sinusoidal int.	0.42256	0.07093	-0.01298

4 RESULTS AND DISCUSSION

4.1 Linear cascade of flat plates

The first test case deals with the one-dimensional model of a linear, infinite-span cascade addressed by reference [11]. The equations of the model can be also obtained from equations (2), (5) and (6) by writing them in Cartesian coordinates and assuming $\frac{\partial}{\partial y} = V_y = 0$, where y is the spanwise coordinate. The main interest of this simple model is the existence of its theoretical solution, though not in closed form, whenever the profile loss effects are neglected, i.e. $\vec{f}_v = 0$.

For the purposes of the test, the flat plate cascade $z = \cos t$ was chosen, with a 20° inlet or incidence angle. Inlet total quantities were set to unity, whereas the back static pressure was set to 0.9. Together with the untreated, discontinuous profile of the tangential velocity, two interpolated profiles were examined in the leading edge region, which was assumed to cover 25% of the plate. The first profile was a linear function of the computational coordinate ξ , on the same equally-spaced mesh as the untreated case. The second profile was obtained by superimposing a complete sinusoid to the first, with a slightly upstream-refined mesh. Both the meshes used 30 grid points for the full plate, but the point number within the leading edge region increased from 8 in the unstretched case to 11 in the stretched case. The authors notice that mesh refinement is detrimental with no leading edge treatment, since the blade force peak in the first cell is roughly proportional to Δx^{-1} .

Moving from the untreated case to the linear interpolation case, and then to the sinusoidal interpolation case, the tangential velocity upstream of the cascade rises closer and closer to the 0.168 theoretical value (Figure 1 right). Since the inflow angle is given, the loss in tangential speed involves an equal loss in axial speed, and then a reduced mass flowrate (first column of Table 1). Consistently with definition (8), the predicted blade load is affected by both the errors on the mass flowrate and tangential speed (second column of Table 1). However, the numerical solution with sinusoidal interpolation approximates the theoretical solution very well, and that obtained with a linear interpolation is still acceptable. The interpolated profiles also allow for prediction of the blade trust, or leading edge suction (third column of Table 1). One-dimensional Euler equations provide, for this quantity, $F_{ix} = -\int_{x_{1e}}^{x_{te}} h(x) f_{ix}(x) dx = \Delta(\dot{m}V_x + p)$, where $h \equiv 1$ with flat plates (cfr. definition (8)). No blade trust is captured by the untreated computation. Figure 2 left compares the tangential blade force distributions obtained in the three cases. The smoothing role of the interpolated profiles on the peak is evident. The correspondent entropy productions are plotted in Figure 2 right.

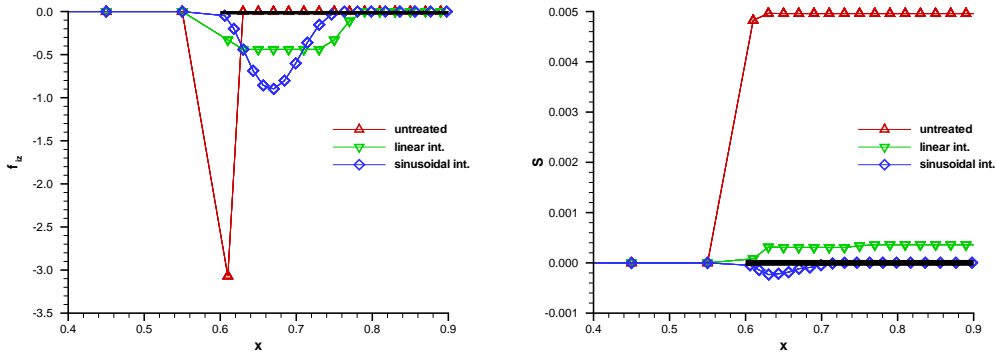


Figure 2: Tangential blade force on the flat plate cascade (left); entropy production (right).

4.2 Three stage compressor

The second test case is simply an example that shows the capabilities of the proposed method, with no other purposes. It deals with an off-design analysis of the three stage compressor of reference [12]. This compressor was designed by means of an inverse method that specifies the load distribution in the blade regions. For rotor rows, the spanwise load distribution was chosen with the purpose to have a given, radially-constant specific work. For each stator row, the same load distribution as the corresponding rotor, but with the opposite sign, was conventionally assumed. In order to have a zero incidence and avoid leading edge discontinuities, the specified tangential component of the inviscid blade force started from zero along all the leading edges. Figure 3 left maps this component on the blade cambersurfaces that were predicted by the inverse solver. The same cambersurface geometry was used in the present test case, with off-design conditions created by increasing the rotational shaft speed from 0.3 to 0.36. The leading edge treatment was approximately applied in the first 30% of each blade region, which took 10 streamwise grid points out of 24 because of the upstream mesh refinement. The interpolation profile for the swirl was similar to the sinusoidal one addressed in Section 4.1 for the tangential velocity.

Figure 3 right maps the tangential component of the inviscid blade force field that was predicted by the present throughflow code in the new conditions. The increase in absolute blade-to-blade angle for the first rotor outlet goes from 1.5° at hub to 3° at tip (Figure 4 left). These values are strictly comparable to those of the incidence angle on the first stator. In off-design conditions, the compressor no longer provides radially-constant total pressure ratio, i.e. specific work. The increase in overall total pressure ratio goes from 8% at hub to 14% at tip (Figure 4 right) and involves a 51% increase in average specific work. No numerical total pressure losses are appreciable in the leading edge regions.

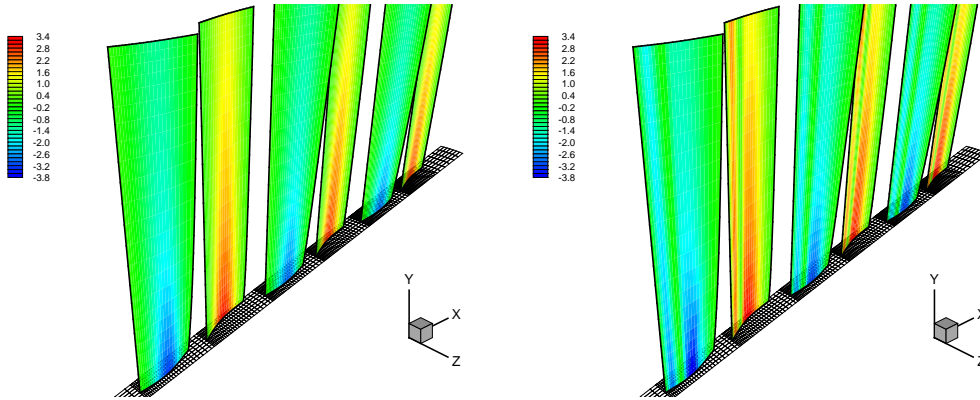


Figure 3: Tangential component of the inviscid blade force specified for design conditions (left) and predicted in off-design conditions (right).

5 CONCLUSIONS

Although a linear interpolation of the swirl can already lead to a satisfactory reduction of the numerical losses, the best results have been obtained by means of a smoother interpolation profile, such as the sinusoidal one. The authors suggest this choice especially for high incidence angles. The interpolation region can cover less than 25-30% of the entire blade, provided that it is still discretized

by at least 10 streamwise grid points. However, the proposed method does not involve any other increase in computational cost, than that due to the mesh refinement immediately downstream of the leading edge.

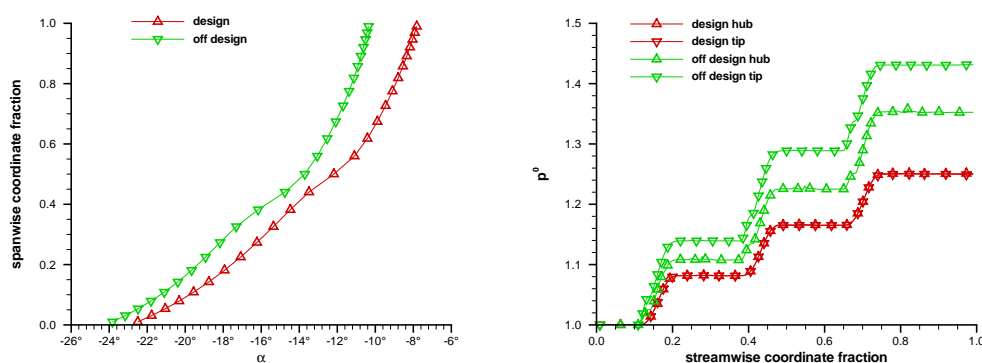


Figure 4: Spanwise distribution of the absolute blade-to-blade angle for the first rotor outlet (left); streamwise distribution of the total pressure along the hub and tip (right).

ACKNOWLEDGEMENTS

This work has been partly funded by Regione Piemonte Italy (Bando Regionale 2004-E57 and Bando Regionale 2006-CORALE) and partly by Avio Group Italy.

References

- [1] Denton J.D. and Dawes W.N., “Computational fluid dynamics for turbomachinery design,” *Proc. IMechE, Part C: J. Mech. Eng. Science*, **213**(2), 107-124 (1999).
- [2] Nigmatullin R.Z. and Ivanov M.J., “The mathematical models of flow passage for gas turbine engines and their components,” *AGARD-LS-198* (1994).
- [3] Baralon, S., Erikson, L.E. and Hall, U., “Validation of a throughflow time-marching finite-volume solver for transonic compressors,” *ASME Paper 98-GT-47* (1998).
- [4] Simon J.F., *Contribution to throughflow modelling for axial flow turbomachines*, PhD diss., Université de Liège (2007).
- [5] Sturmayer A. and Hirsch Ch., “Throughflow model for design and analysis integrated in a three-dimensional Navier-Stokes solver,” *Proc. IMechE, Part A: J. Power and Energy*, **213**(4), 263-273 (1999).
- [6] Yao Z. and Hirsch Ch., “Throughflow model using 3D Euler or Navier-Stokes solvers,” in *Turbomachinery-Fluid Dynamic and Thermodynamic Aspects*, VDI Berichte 1185, Verein Deutscher Ingenieure, Düsseldorf (1995).
- [7] Damle, S.V., Dang, T.Q. and Reddy, D.L., “Throughflow method applicable for all flow regimes,” *Trans. ASME J. Turbomachinery*, **119**, 256-262 (1997).

- [8] Rosa Taddei S. and Larocca F., “Axisymmetric design of axial turbomachines: an inverse method introducing profile losses,” *Proc. IMechE, Part A: J. Power and Energy*, **222**(6), 613-621 (2008).
- [9] Pandolfi M., “A contribution to the numerical prediction of unsteady flows,” *AIAA J.*, **22**(5), 602-610 (1984).
- [10] Harten, A., Engquist, B., Osher, S. and Chakravarthy, S.R., “Uniformly high order accurate essentially non-oscillatory schemes, III,” *J. Comp. Phys.*, **71**, 231-303 (1987).
- [11] Zannetti L. and Pandolfi M., *Inverse design technique for cascades*, NASA-CR-3836 (1984).
- [12] Bena, C., Larocca, F. and Zannetti, L., “Design of multi-stage axial flow turbines and compressors,” in *Proc. IMechE 3rd European Conference on Turbomachinery*, London, 635-644 (1999).

APPENDIX: LIST OF SYMBOLS

E, H, S	specific energy, specific enthalpy, entropy
\vec{f}	volume force
F_{ix}, F_{iz}	blade thrust, blade load
δ, h, n	blade thickness, blockage factor, blade number
$\vec{i}, \vec{j}, \vec{k}$	axial unit vector, radial unit vector, tangential unit vector
m, r, x	meridional streamline coordinate, radial coordinate, axial coordinate
\dot{m}	mass flowrate
Ma, \vec{V}	Mach number, flow velocity
p, ρ	pressure, density
t	time
z, ϑ	tangential coordinate
α	blade-to-blade flow angle
γ	specific heat ratio ($\gamma = 1.4$)
η, ξ	computational coordinates
ω	rotational shaft speed

Subscripts

i, v	inviscid, viscous
le, te	leading edge, trailing edge
m, r, x	meridional component, radial component, axial component
rel	relative quantities
z, ϑ	tangential component

Superscripts

0	total quantities
---	------------------